Journal of Materials Chemistry C

Accepted Manuscript

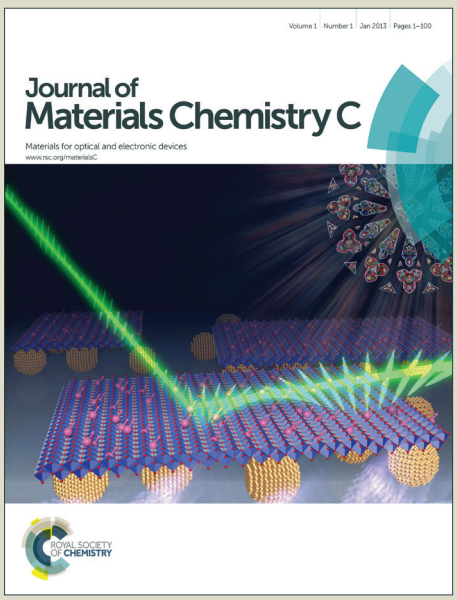

ROYAL SOCIETY OF CHEMISTRY

www.rsc.org/materialsC

Cite this: DOI: 10.1039/c0xx00000x

www.rsc.org/xxxxxx

ARTICLE TYPE

The Structure, Photoluminescence and Thermal Properties of Ce^{3+}, Mn^{2+} Co-doped Phosphosilicate $Sr_7La_3[(PO_4)_{2.5}(SiO_4)_3(BO_4)_{0.5}](BO_2)$ Emission-tunable Phosphor

Zhipeng Ci,[*a] Qisheng Sun[a], Mengxing Sun[a], Xiaojing Jiang[a], Shengchun Qin[a], Yuhua Wang[*a]

Received (in XXX, XXX) XthXXXXXXXXX 20XX, Accepted Xth XXXXXXXXX 20XX
DOI: 10.1039/b000000x

ABSTRACT

A single phase emission-tunable Ce^{3+}, Mn^{2+} co-doped phosphosilicate $Sr_7La_3[(PO_4)_{2.5}(SiO_4)_3(BO_4)_{0.5}](BO_2)$ phosphor was synthesized by the solid-state reaction. Commonly blue and orange broad band emissions from Ce^{3+} and Mn^{2+} are detected under the excitation of 351 nm. Combined with the crystallographic data from the Rietveld refinements, the blue and orange bands can be well fitted by Gauss Function in accordance with the three different sites. By adjusting the radio of Ce^{3+}/Mn^{2+}, the warm-white light is generated with the correlated color temperature from 2500-4500 K. The mechanism of energy transfer between Ce^{3+} and Mn^{2+} has been also carefully investigated by the photoluminescence spectra and decay times. The thermal properties from 20 to 250 ℃ present an abnormal changing trend. With the increase of temperature, the Ce^{3+} or Mn^{2+} single-doped samples show excellent thermal properties, while for the Ce^{3+} and Mn^{2+} co-doped sample, the thermal properties reveal serious degeneration. Based on the configurational coordinate diagram, an underlying mechanism of thermal quenching is proposed and can reasonably explain the phenomenon. What is more, the mechanism could be helpful for the understanding of the thermal properties of multiple activators co-doped phosphors as reference.

1. Introduction

In the last few decades, inorganic luminescent materials/phosphors have undergone a rapid development because of a wide range of applications for white-light emitting diodes (LEDs), cathode ray tubes (CRTs), vacuum fluorescent displays, plasma display panels, fluorescent lamp, X-ray imaging scintillators and field emission displays (FEDs), etc. [1-5] Especially the phosphors with high efficiency, low cost and environment friendly more attract widespread attention in these days, such as phosphates, silicates and borates. [6-16] In order to meet the demands of practical application, generally, two more phosphors are required to use in the production of the device. However, the strategy using multi-phosphors usually suffers from two problems of different light output degradation rates leading to the color aberration and the trade-off in luminous efficiency attributed to re-absorption among the different phosphors. [17] A useful solution is to develop a emission-tunable phosphor through the co-doping sensitizer and activator into a crystalline matrix, such as Eu^{2+} to Mn^{2+}, [18, 19] Ce^{3+} to Tb^{3+}, [20, 21] Ce^{3+} to Eu^{2+} or Ce^{3+} to Mn^{2+} [22-25].

As is well known, the Ce^{3+} with the 4*f* configuration shows efficient broad band luminescence due to the 4*f*-5*d* parity allowed electric dipole transition, and the Ce^{3+} has a larger Stokes shift than that of the other rare earth ions, owing to the extended radial wavefunctions of the 5*d* states. [26] Moreover, the Ce^{3+} also acts as a good sensitizer, transferring a part of its energy to activator ions. [27] The transition metal ion Mn^{2+} can give a broad emission band in the visible range owing to the *d*-*d* transition, but it is forbidden and difficult to pump. So the emission of Mn^{2+} is normally excited by the energy transfer (ET) from the host or the sensitizer. [28] As a promising sensitizer for Mn^{2+}, Ce^{3+} has been widely used in many Mn^{2+}-doped hosts to improve the emission intensity of Mn^{2+}.

Apatite structure is an important branch of phosphate system, which are represented by the general formula $M_{10}(ZO_4)_6X_2$ with M=Ca^{2+}, Ba^{2+}, Mg^{2+}, Sr^{2+}, Pb^{2+}, Na^{+}, K^{+}, La^{3+}, etc.; Z=P^{5+}, As^{5+}, V^{5+}, Si^{4+}, etc.; and X=F^{-}, Cl^{-}, Br^{-}, I^{-}, OH^{-}, O^{2-}, etc., and shows the wide range of tolerance of this structure type to chemical substitutions. [29-31] In addition, there are also reports on linear $[BO_2]^{-}$ groups taking the position of X [32, 33]. $Sr_{10}(PO_4)_{5.5}(BO_4)_{0.5}(BO_2)$ was first discovered by Chen, etc. [34] in 2010. $Sr_{10}(PO_4)_{5.5}(BO_4)_{0.5}(BO_2)$ is a derivative of the apatite crystal structure. Sr^{2+} occupies the Wyckoff positions 2d (Sr_1, Sr_2) and 6g (Sr_3). $[PO_4]^{3-}$ tetrahedra (6g) are partially replaced by $[BO_4]^{5-}$ groups. The linear $[BO_2]^{-}$ units are located within the channels formed by Sr_3 ions and running along the three-fold inversion axis. The space group symmetry of the title compound is reduced to $P\bar{3}$ by displacement of the $[(P+B)O_4]$ tetrahedra destroying the mirror plane characteristic for the parent apatite crystal structure (P63/m), which is found for strontium fluorapatite $Sr_{10}[PO_4]_6F_2$. In many researches, $[SiO_4]^{4-}$ could replace $[PO_4]^{3-}$ to form a solid solution, such as $Ca_5(PO_4)_2SiO_4$, $Sr_{3.5}Y_{6.5}O_2(PO_4)_{1.5}(SiO_4)_{4.5}$, $Ca_3Gd_7(PO_4)(SiO_4)_5O_2$ [35-37]. The doping of $[SiO_4]^{4-}$ group would cause the distortion of the structure, further influence the crystal field and change the Nephelauxetic Effect when the rear earth ions are doped. Thereby, it will probably cause the diversity of luminescence properties. In this work, we have synthesized a series of phosphors $(Sr_{0.7-y}La_{0.3-x})_{10}[(PO_4)_{2.5}(SiO_4)_3(BO_4)_{0.5}](BO_2)$ (SPSB): $x$$Ce^{3+}$, $y$$Mn^{2+}$ ($0.001 \le x \le 0.04$, $0.02 \le y \le 0.16$) by the solid-state

reaction method. The structure, photoluminescence and thermal properties as well as the ET phenomenon between the sensitizer and activator are investigated in detail.

2. Experimental

2.1 Materials and synthesis

All the powder samples were synthesized by the traditional solid-state reaction method. The starting materials were $SrCO_3$ (A.R.), $(NH_4)_2HPO_4$ (A.R.), SiO_2 (A.R.), H_3BO_3 (A.R.), $MnCO_3$ (A.R.), La_2O_3 (4N), $Ce(NO_3)_3{\cdot}6H_2O$ (4N) and Eu_2O_3 (4N). The stoichiometric raw materials were ground thoroughly in an agate mortar and then heated to 773 K in air for 5h. Subsequently the preheated mixture was ground again and fired to 1533 K for 8 h in an alumina crucible under N_2-H_2 (10%) atmosphere in horizontal tube furnaces. Finally the as-synthesized samples were slowly cooled to the room temperature inside the tube furnace under H_2-N_2 flow.

2.2 Measurements and characterization

The crystal structures of the synthesized samples were identified by using a Rigaku D/Max-2400 X-ray diffractometer with Ni filtered CuKa radiation (XRD). Diffuse reflection spectra were obtained by a UV/visible spectrophotometer (Perkin-Elmer Lambda 950) using $BaSO_4$ as a reference in the range of 240-700 nm. The photoluminescence (PL), photoluminescence excitation (PLE) spectra and decay curves of the samples were measured using an FLS-920T fluorescence spectrophotometer equipped with a 450 W Xe light source, Xe Flash Lamp and ns pulsed hydrogen lamp. The quantum efficiency was measured by a Fluorlog-3 spectrofluorometer equipped with a 450 W xenon lamp (Horiba Jobin Yvon). All of the measurements were performed at room temperature. Thermal quenching was tested using a heating apparatus (TAP-02) in combination with PL equipment.

3. Results and discussion

3.1 Crystal Structure of SPSB

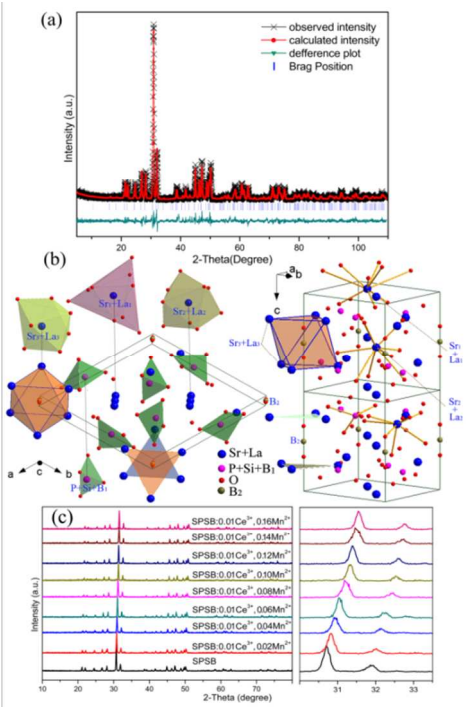

Figure 1 (a) Experimental (crosses), calculated (red solid line) and difference (bottom) results of XRD refinement of SPSB host; (b) The structure diagram of SPSB according to the refinement; (c) The XRD patterns of the samples SPSB and SPSB: $0.01Ce^{3+}$, xMn^{2+} ($0.02 \le x \le 0.16$).

Figure 1(a) shows the results of Rietveld refinement for SPSB implemented with the crystallographic information files identified by previous reports [34]. The black crosses and red solid line depict the observed and calculated patterns, respectively; the as-obtained goodness of fit parameter $\chi^2 = 2.098$ and $R_{wp} = 10.6\%$ and $R_p = 7.8\%$ can ensure the phase purity. The compound crystallizes in a trigonal crystal system with space group $P\bar{3}$ (No. 147), and its cell parameter is $a = b = 9.755(6)$ Å, $c = 7.298(2)$ Å. The detailed crystallographic data of SPSB are listed at Table 1 and 2. Figure 1(b) presents the crystal structure of SPSB. SPSB is a derivative of the apatite crystal structure. SL (SL = 7/10Sr +3/10 La) ions occupy the Wyckoff positions 2d (SL_1, SL_2) and 6g (SL_3). SL_1 and SL_2 are nine-fold coordinated (d(SL_1-O)= 2.3697 Å - 3.7899 Å, d(SL_2-O)= 2.7372 Å - 3.1670 Å) with an average distance of 2.9144 Å and 2.9017 Å, respectively. SL_3 is surrounded by seven oxygen atoms forming a distorted pentagonal bipyramid (d(SL_3-O)= 2.2597 Å - 2.8157 Å) with an average distance of 2.5051 Å. P, Si and partial B (B_1) ions occupy the Wyckoff positions 6g and form a seriously distorted tetrahedra with four oxygen atoms. The Z-O distances (Z=5/12 P + 1/2 Si + 1/12 B_1) vary from 1.4331 Å to 2.0927 Å with an average Z-O distance of 1.7044 Å. The reminding B (B_2) ions occupy the Wyckoff positions 1b and form the linear BO_2^- units, which are located within the channels formed by SL_3 ions. Figure 1(c) shows that the XRD patterns of the samples SPSB and SPSB: $0.01Ce^{3+}$, xMn^{2+} ($0.02 \le x \le 0.16$). All the observed diffraction peaks are well indexed to that of SPSB and no second phase is observed, indicating that the doping ions do not cause significant changes in the host structure. Since the radius of Mn^{2+} is smaller than that of Sr^{2+}, La^{3+} and Ce^{3+}, with the doping of Mn^{2+}, the diffraction peaks of the SPSB: $0.01Ce^{3+}$, xMn^{2+} samples show an obvious shift to larger 2θ angles compared to that of the pure SPSB.

Table 1 Crystallographic data of SPSB determined by the Rietveld refinement of power XRD data at the room temperature.

Atom	Wyck.	*x/a*	*y/b*	*z/c*
SL_1	2*d*	1/3	2/3	0.00180
SL_2	2*d*	1/3	2/3	0.51240
SL_3	6*g*	0.24410	-0.01690	0.25100
P	6*g*	0.39930	0.36780	0.25080
Si	6*g*	0.39930	0.36780	0.25080
B_1	6*g*	0.39930	0.36780	0.25080
O_1	6*g*	0.34410	0.47890	0.24060
O_2	6*g*	0.58050	0.48800	0.15830
O_3	6*g*	0.19070	0.17200	0.15620
O_4	6*g*	0.35300	0.25820	0.42820
O_5	2*c*	0	0	0.34570
B_2	1*b*	0	0	1/2

Space group: $P\bar{3}$ (No. 147), V = 694.5823(3) Å^3, $a = b = 9.755(6)$ Å, $c = 7.298(2)$Å, $R_p = 7.8\%$, $R_{wp} = 10.6\%$, $\chi^2 = 2.098$

Table 2 Selected interatomic distances in the crystal structure of SPSB.

Atom contacts		Å	Atom contacts		Å
SL_1	O_1	2.5687	SL_2	O_4	2.8015
SL_1	O_1	2.5683	SL_2	O_4	2.8005
SL_1	O_1	2.5680	SL_2	O_4	2.8012
SL_1	O_2	2.3698	SL_3	O_1	2.8157
SL_1	O_2	2.3697	SL_3	O_2	2.3744
SL_1	O_2	2.3899	SL_3	O_3	2.2597
SL_1	O_2	3.7891	SL_3	O_3	2.3621
SL_1	O_2	3.7892	SL_3	O_4	2.6744
SL_1	O_2	3.7899	SL_3	O_4	2.4865
SL_2	O_1	2.7378	SL_3	O_5	2.5629
SL_2	O_1	2.7375	Z^*	O_1	1.4331
SL_2	O_1	2.7372	Z^*	O_2	1.6979
SL_2	O_2	3.1670	Z^*	O_3	2.0927
SL_2	O_2	3.1665	Z^*	O_4	1.5939
SL_2	O_2	3.1664	B_2	O_5	1.1261

SL = 7/10Sr +3/10 La, Z^*=5/12 P + 1/2 Si + 1/12 B_1

3.2 Photoluminescence properties analysis

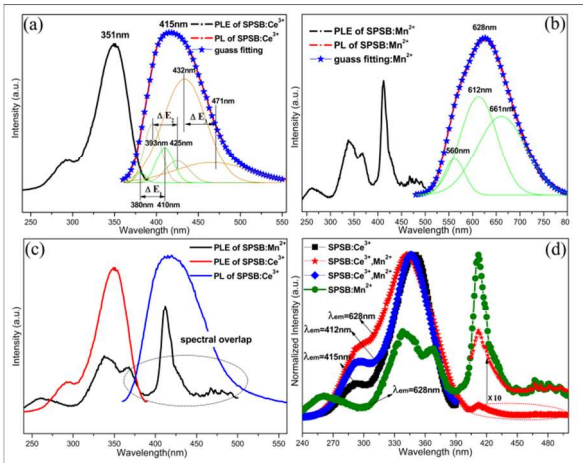

Figure 2 (a) The PL spectrum (λ_{ex} = 351 nm) and PLE spectrum (λ_{em} = 415 nm) of SPSB: 0.01Ce^{3+}; (b) The PL spectrum (λ_{ex} = 410 nm) and PLE spectrum (λ_{em} = 628 nm) of SPSB: 0.08Mn^{2+}; (c) The overlap between the PLE spectrum of SPSB: 0.08Mn^{2+} and the PL spectrum of SPSB: 0.01Ce^{3+}; (d) the PLE spectra of typical samples monitored at different emission peaks.

Figure 2(a) and (b) show the PL and PLE spectra for SPSB: 0.01Ce^{3+} (a) and SPSB: 0.08Mn^{2+} (b). The PLE spectrum of SPSB: 0.01Ce^{3+} monitored at 415 nm extends from 240 to 390 nm with two distinct bands peaking at 293 and 351 nm attributed to the 4*f*-5*d* transition of Ce^{3+}, which indicates that the phosphor can be effectively excited by the UV light. The emission spectrum shows an asymmetric broadband characteristic of Ce^{3+}. Considering that there are three different cationic sites in SPSB (as illustrated in Figure. 1(b)), then we take the Gaussian fitting algorithm and find that the curve can be well fitted into six emission bands centered at 380 and 410 nm, 393 and 425 nm, 432 and 471 nm, with an energy difference of 1925 cm^{-1}, 1915 cm^{-1} and 1916 cm^{-1}, respectively, which is close to the theoretical energy different value of Ce^{3+} (~2000 cm^{-1}) [38]. So the six peaks can be justifiably assigned to the 5*d*-4*f* ($^2F_{5/2}$, $^2F_{7/2}$) emissions of Ce^{3+} occupying three SL sites. Generally, the bond length (*R*) of SL-O determines the crystal field strength (*Dq*), and then the crystal field strength affects the positions of the emission peaks significantly. The average distances of SL_1-O, SL_2-O and SL_3-O are 2.9144 Å, 2.9017 Å and 2.5051 Å, resulting from the Rietveld refinement results. According to the equation $Dq \propto 1/R^5$, [39] the bands peaking at 380 and 410 nm, 393 and 425 nm, 432 and 471nm could be assigned to Ce^{3+} occupying SL_1, SL_2, SL_3 sites, respectively, which is identify with that resulted from the equation: [40]

$$E(cm^{-1}) = Q^*\left[1-\left(\frac{V}{4}\right)^{\frac{1}{V}}\right]\times 10^{\frac{-(nEar)}{80}} \qquad (1)$$

where *E* is the position for the Ce^{3+} emission peak, *Q** is the position in energy for the lower 5*d* band edge, *V* is the valence of the Ce^{3+}, *n* is the number of anions in the immediate shell about the Ce^{3+}, *Ea* is the electron affinity of the anions (eV), and *r* is the radius of the host cation replaced by the Ce^{3+} (Å). *Ea* is a constant in the same host and *V* = 3, so the value of *E* is directly proportional to the product of *n* and *r*. The PLE and PL spectra of SPSB: xCe^{3+} ($0.001 \le x \le 0.04$) with the increase of Ce^{3+} are shown in Figure S1 of the Supporting Information. The optimal emission intensity of the samples is at *x* = 0.01. Thereby, the Ce^{3+}-doped concentration in SPSB: xCe^{3+}, yMn^{2+} is fixed as *x* = 0.01. In Figure 2(b), the PLE spectrum of SPSB: 0.08Mn^{2+} monitored at 628 nm consists of several weak bands in the UV and visible regions, which are assigned to the spin-forbidden transitions in the $3d^5$ electron configurations of the Mn^{2+}. The PL spectrum shows an orange emission band, which can be well fitted by three Gaussian peaks centered at 560, 612 and 661 nm, which attribute to the $^4T_1 \rightarrow {}^6A_1$ transition of $3d^5$ level of Mn^{2+} occupied the three different sites. Figure 2(c) presents obvious overlap between the PLE spectrum of Mn^{2+} and the PL spectrum of Ce^{3+}, it implies that the effective resonance-type ET could take place from Ce^{3+} to Mn^{2+}. Monitored at 415, 412 and 628 nm, the PLE spectra shapes of typical samples are very similar in Figure 2(d). It indicates that the excitation of Ce^{3+} contributes to the emitting of Mn^{2+}, and further proves that the efficiency ET occurs. Therefore, it is possible to obtain emission-tunable light by adjusting the radio of Ce^{3+}/Mn^{2+} in SPSB.

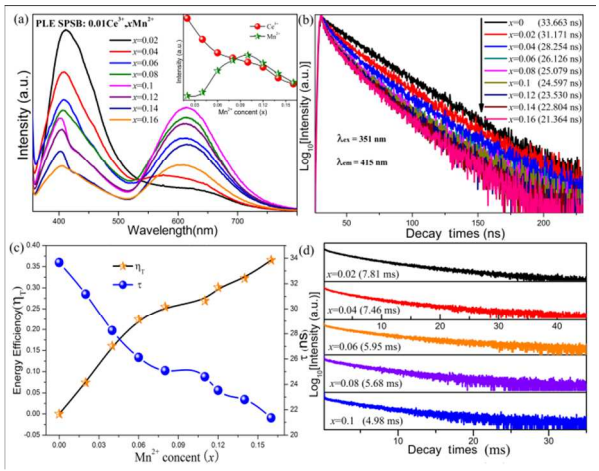

Figure 3 (a) The PL spectra of SPSB: 0.01Ce^{3+}, $x$$Mn^{2+}$ (0.02 ≤ x ≤0.16) under the excitation of 351 nm and the relative intensity of the Ce^{3+} and Mn^{2+} emission bands (b) Decay curves of Ce^{3+} for SPSB: 0.01Ce^{3+}, $x$$Mn^{2+}$ monitored at 415 nm; (c) The variation of η_T and τ with the increasing Mn^{2+} x; (d) Decay curves of Mn^{2+} for SPSB: 0.01Ce^{3+}, $x$$Mn^{2+}$ monitored at 628 nm.

In Figure 3(a), the PL spectra of SPSB: 0.01Ce^{3+}, $x$$Mn^{2+}$ (0.02 ≤ x ≤ 0.16) excited at 351 nm exhibit not only the blue emission of Ce^{3+} but also the red emission of Mn^{2+}. As the increase of Mn^{2+} with the fixed Ce^{3+} concentration, the intensities of the blue band decrease gradually while those of the red band increase. These results also support the occurrence of ET from Ce^{3+} to Mn^{2+}. When the concentration of Mn^{2+} x is up to 0.1the emission intensity of Mn^{2+} reaches maximum. According to the equation, [41] the critical distance Rc for ET from the Ce^{3+} to Mn^{2+}can be estimated:

$$R_c \approx 2\left(\frac{3V}{4\pi x_c N}\right)^{1/3} \qquad (2)$$

Where V is the volume of the unit cell, x_c is the critical concentration, and N is the number of available sites for the dopant in the unit cell. In our case, N = 10, V = 694.49 Å^3. The critical concentration (x_c), at which the luminescence intensity of Ce^{3+} is one half of that in the sample in the absence of Mn^{2+}, is 0.1. Therefore, the critical distance (R_c) is calculated to be 10.99 Å, which indicates the energy transfer is not via exchange interaction mechanism but electric multipolar interaction [42, 43]. To further understand the process of energy transfer, the PL decay curves of Ce^{3+} excited at 351 nm are measured and depicted in Figure 3(b). We can see that the decay curves of the Ce^{3+} emission deviate slightly from a single exponential rule at lower Mn^{2+} content and the deviations become more evident with the increase of the Mn^{2+} concentration. The effective lifetimes of the decay curves for Ce^{3+} emission can be evaluated using the equation [44]:

$$\tau = \frac{\int_0^\infty tI(t)dt}{\int_0^\infty I(t)dt} \qquad (3)$$

The calculated decay times are determined to be 33.663, 31.171, 28.254, 26.126, 25.179, 24.597, 23.530, 22.804, 21.364 ns in Figure 3 (b). According to Dexter's formulation [45], the ET rate is given by:

$$P(R) \propto \frac{Q_A}{R^b \tau_D} \int \frac{f_D(E)F_A(E)}{E^c} dE \qquad (4)$$

Where τ_D is the decay time of the donor emission, Q_A is the total absorption cross section of the acceptor ion, R is the distance between the donor and the acceptor, and b and c are parameters dependent on the type of ET. The probability functions $f_D(E)$ and $F_A(E)$ represent the observed shapes of the donor emission band and the acceptor absorption band, respectively. Thus, according to Eq. (4), the energy transfer rate P is in inverse proportion to the decay time τ_D. The decay lifetime of the Ce^{3+} decreases monotonically with the increase of Mn^{2+}, which further supports the ET from the Ce^{3+} to Mn^{2+}. The energy transfer efficiency $\eta_{Ce\text{-}Mn}$ can be expressed by:

$$\eta = 1 - \frac{\tau_s}{\tau_{s0}} \qquad (5)$$

Where τ_{S0} is the lifetime of the Ce^{3+} in the absence of the Mn^{2+} and τ_S is the lifetime of the Ce^{3+} in the presence of the Mn^{2+}. The decay lifetime values are used for calculation, and the results are presented in Figure 3(c). The Figure 3(d) shows the decay times depended on Mn^{2+} contents monitored at 628 nm. The decay times τ are calculated to be 7.81 (x = 0.02), 7.46 (x = 0.04), 5.95 (x = 0.06), 5.68 (x = 0.08) and 4.98 (x = 0.1) ms with the Mn^{2+} contents from 2% to 10%, respectively. It obviously observed that the decay times gradually decrease and when the Mn^{2+} content x reaches 6%, the decay time sharply declines, which indicates that the energy transfer between $Mn^{2+}$and Mn^{2+} might occur. Thereby, the quenching concentration is confirmed at 6% by the changes of decay times.

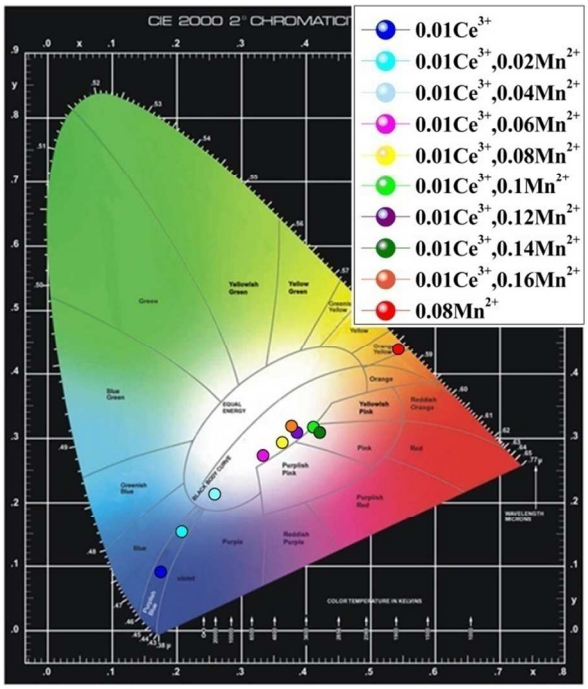

Figure 4 The Commission International de L' Eclairage (CIE) chromaticity coordinates of the samples SPSB: 0.01Ce^{3+}, SPSB: 0.08Mn^{2+} and SPSB: 0.01Ce^{3+}, $x$$Mn^{2+}$ (0.02 ≤ x ≤ 0.16).

Figure 4 shows the CIE chromaticity coordinates of the samples calculated based on their corresponding PL spectra. With increasing Mn^{2+} concentration, the emission color locates at the blue, warm white, orange region with the chromaticity coordinates changing from (0.177, 0.095) to (0.375, 0.289) to (0.55, 0.44). The chromaticity coordinates and correlated color temperature (CCT) of optimal sample SPSP: 0.01Ce^{3+}, 0.08Mn^{2+} are (0.375, 0.289) and 3114 K, respectively, and the quantum efficiency is measured to be 28.7%. It indicates the SPSB: Ce^{3+}, Mn^{2+} phosphor could be regarded as a kind of single phase emission-adjusted phosphor. The particular data of CIE and CCT are listed in Table 3.

Table 3 The detailed data of color, CIE, CCT of SPSB: 0.01Ce^{3+}, SPSB: 0.08Mn^{2+}, SPSB: 0.01Ce^{3+}, $x$$Mn^{2+}$ ($0.02 \leq x \leq 0.16$) and blue chips +YAG

	Samples compositions	color	CIE		CCT (K)
			x	y	
1	SPSB:0.01Ce^{3+}	blue	0.177	0.095	-
2	SPSB:0.08Mn^{2+}	orange	0.55	0.44	-
3	SPSB:0.01Ce^{3+},0.02Mn^{2+}	blue	0.211	0.158	-
4	SPSB:0.01Ce^{3+},0.04Mn^{2+}	blue white	0.257	0.210	1488
5	SPSB:0.01Ce^{3+},0.06Mn^{2+}	warm white	0.349	0.275	4217
6	SPSB:0.01Ce^{3+},0.08Mn^{2+}	warm white	0.375	0.289	3114
7	SPSB:0.01Ce^{3+},0.10Mn^{2+}	warm white	0.424	0.323	2263
8	SPSB:0.01Ce^{3+},0.12Mn^{2+}	warm white	0.406	0.315	2547
9	SPSB:0.01Ce^{3+},0.14Mn^{2+}	warm white	0.427	0.323	2208
10	SPSB:0.1Ce^{3+},1.6Mn^{2+}	warm white	0.392	0.314	2928
11	blue chips +YAG	cold white	0.291	0.300	5610

3.3 Thermal properties analysis

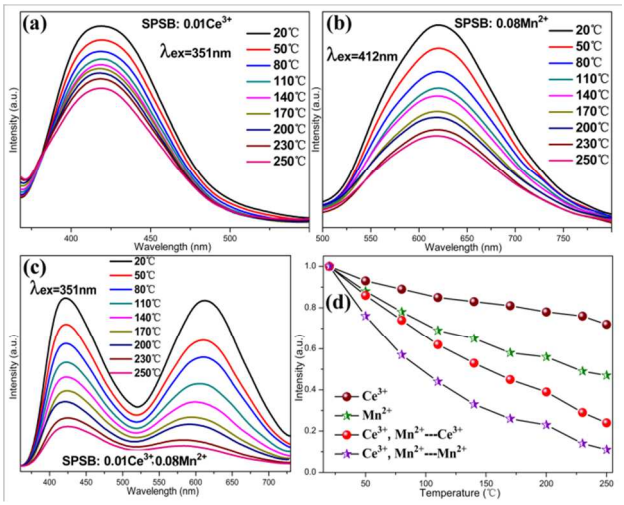

Figure 5 The PL spectra of (a) SPSB: 0.01Ce^{3+}, (b) SPSB: 0.08Mn^{2+}, (c) SPSB: 0.01Ce^{3+}, 0.08Mn^{2+} phosphors under various temperatures, (d) The dependence of normalized PL intensities on temperature for phosphors.

A comprehensive understanding of the thermal quenching of phosphors in the process of the phosphors application is indispensable because many devices suffer from thermal problems. Numerous investigations have discussed the thermal quenching behaviors. [46-50] Two competing factors are in prevail, one is the activation energy of non-radiative relaxation, the other is the rate of temperature-induced direct tunneling, which prevents emissive transition between the different activator ions excited state and the ground state in host. [51]

The temperature dependent PL spectra of SPSB: 0.01Ce^{3+}, SPSB: 0.08Mn^{2+} and SPSB: 0.01Ce^{3+}, 0.08Mn^{2+} excited at 351 nm are shown in Figure 5(a), (b) and (c), respectively. The thermal quenching behavior is measured from 20 to 250 ℃. With the increasing temperature, the emission intensities of all samples gradually decline. The emission intensity of SPSB: 0.01Ce^{3+}, SPSB: 0.08Mn^{2+} at 250 ℃ is 72.1% and 47.3% of their initial intensities at 20 ℃. When Ce^{3+} and Mn^{2+} are co-doped into SPSB host, the thermal properties rapidly decline. For the sample SPSB: 0.01Ce^{3+}, 0.08Mn^{2+}, the PL intensities of Ce^{3+} and Mn^{2+} drop to 24.6% and 12.8% of those at 20 ℃, which indicates that the co-doping of Ce^{3+} and Mn^{2+} cause a serious decrease in thermal properties (as seen in Figure 5 (d)). The phenomenon could be explained by the configurational coordinate diagram in Figure 6. In order to simplify the discussion, we assume the excited states and ground states of Ce^{3+} and Mn^{2+} can be expressed by only one curve. The curve g_1 and g_2 are the ground states of Mn^{2+} and Ce^{3+}, and the curves e_1 and e_2 are the excited states of Mn^{2+} and Ce^{3+}, respectively. A and B are the lowest positions of the e_1 and e_2. C and D are the crossing points of g_1, g_2 and e_1, e_2, respectively. M is the crossing point of e_1 and g_2. P is the crossing point of e_2 and g_2. ΔE_1, ΔE_2 and ΔE_3, ΔE_4 are the energy differences of P to B, C to A, D to B and M to A, respectively. Under the excitation of the UV light, the electrons are excited to the excited states from g_1, g_2 to e_1, e_2. At the room temperature, for the samples SPSB: 0.08Mn^{2+} and SPSB: 0.01Ce^{3+}, most of the electrons return to the ground states along the red way ① to bring out the orange emission of Mn^{2+} and the blue way ② to obtain the blue emitting of Ce^{3+}. For the sample SPSB: 0.01Ce^{3+}, 0.08Mn^{2+}, besides the ways ① and ②, the electrons of the Ce^{3+} exited state would very likely overcome the energy barrier ΔE_1 under the electron-phonon coupling, and transfer energy to Mn^{2+} along the green way ③, resulting in the enhancing of the Mn^{2+} emission intensity. With the increase of temperature, for the samples SPSB: 0.08Mn^{2+} and SPSB: 0.01Ce^{3+}, more electrons could overcome the energy barrier ΔE_2 and ΔE_3, and return to the ground along the orange way ④ and the cyan way ⑤ from the crossing points C and D due to the stronger electron-phonon coupling. For the sample SPSB: 0.01Ce^{3+}, 0.08Mn^{2+}, more electrons of the excited state e_2 would transfer to the Mn^{2+} excited state e_1 under the stronger phonon vibration, which results in the worse thermal properties of Ce^{3+} in SPSB: 0.01Ce^{3+}, 0.08Mn^{2+} than that in SPSB: 0.01Ce^{3+}. However, although the energy transfer process from Ce^{3+} to Mn^{2+} is strengthened, the emission intensity of Mn^{2+} is not enhanced. This may be due to the smaller ΔE_4, resulting from the lower position of the crossing point M than that of the crossing point C. With increasing temperature, more electrons of the excited state of Mn^{2+} could return to the ground along the pink way ⑥, and this process also decreases the possibility of the back tunneling of electrons from the Mn^{2+} excited state e_1 to the Ce^{3+} excited e_2, and thereby leads to the rapid degradation of the thermal properties of Ce^{3+} and Mn^{2+} in the sample SPSB: 0.01Ce^{3+}, 0.08Mn^{2+}.

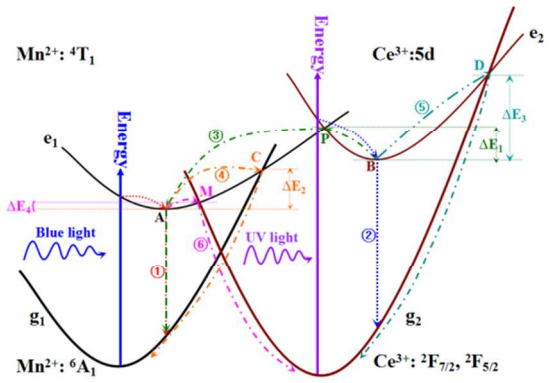

Figure 6 The configurational coordinate diagram of the ground states of Ce^{3+}, Mn^{2+} and the excited states of Ce^{3+}, Mn^{2+}.

Conclusions

In summary, a simple solid-state route was adopted to fabricate a series of phosphosilicate phosphors SPSB: Ce^{3+}, Mn^{2+}. Their crystal structure, photoluminescence properties, decay times, CIE index, CCT, and thermal properties are discussed. The luminescence analysis demonstrates that the phosphors SPSB: Ce^{3+}, Mn^{2+} can be efficiently excited by the UV light from 240 to 390 nm, and simultaneously emit the blue light from Ce^{3+} and the orange light from Mn^{2+}. By adjusting the radio of Ce^{3+}/Mn^{2+}, the warm white light with CCT from 2500 to 4500 K can be obtained, which is suitable for the indoor lighting. The spectral characteristic and decay times indicate that the efficient ET occurs between Ce^{3+} and Mn^{2+}. With the increase of temperature, the emission intensities of all samples gradually decline. The emission intensities of SPSB: $0.01Ce^{3+}$ and SPSB: $0.08Mn^{2+}$ at 250 ℃ are 72.1% and 47.3% of those at 20 ℃, respectively, which indicates that Ce^{3+} or Mn^{2+} single-doped SPSB shows excellent thermal properties. However, when the Ce^{3+} and Mn^{2+} are co-doped into the host SPSB, the thermal properties rapidly degrade. The PL intensities of Ce^{3+} and Mn^{2+} in SPSB: $0.01Ce^{3+}$, $0.08Mn^{2+}$ drop to 24.6% and 12.8% of those at 20 ℃. According to the configurational coordinate diagram, we propose an underlying mechanism of thermal quenching and reasonably elucidate the abnormal degradation phenomenon. The results imply the mechanism could be useful for the discussion of the thermal properties of multiple activators co-doped phosphors as reference.

Acknowledgments

This work was supported by National Natural Science Funds of China (No. 51302121) and the Research Fund for the Doctoral Program of Higher Education (No. 20120211130003).

Notes and references

[a] *Department of Materials Science, School of Physical Science and Technology, Lanzhou University, Lanzhou 730000, China, Fax.: +86-931-8913554 (Office), Tel.: +86-931-8912772 (Office), E-mail: cizhp@lzu.edu.cn.*

†Electronic Supplementary Information (ESI) available: Figure S1 shows the PLE spectrum of SPSB: $0.01Ce^{3+}$ and PL spectra of SPSB: xCe^{3+} ($0.001 \le x \le 0.04$) with the increase of Ce^{3+}; The inset shows the PL intensities of SPSB: xCe^{3+} as a function of the Ce^{3+} content x. See DOI: 10.1039/b000000x/

1 G.Wakefield, E. Holland, P. J. Dobson, J. L. Hutchison, *Adv. Mater.*, 2001, **13**, 1557.
2 R. J. Xie, N. Hirosaki, K. Sakuma, Y. Yamamoto, M. Mitomo, *Appl. Phys. Lett.*, 2004, **84**, 5404.
3 W. B. Im, S. Brinkley, J. Hu, A. Mikhailovsky, S. P. DenBaars, R. Seshadri, *Chem. Mater.*, 2010, **22**, 2842.
4 Q. Dai, M. E. Foley, C. J. Breshike, A. Lita, G. F. Strouse, *J. Am.Chem. Soc.*, 2011, **133**, 15475.
5 A. M. Srivastava, R. G. Chandran, M. V. Shankar, *Chem. Mater.*, 2006, **18**, 3314.
6 M. M. Shang, G. G. Li, D. L. Geng, D. M. Yang, X. J. Kang, Y. Zhang, H. Z. Lian, J. Lin, *J. Phys. Chem. C*, 2012, **116**, 10222.
7 R. Y. Mi, C. L. Zhao, Z. G. Xia, *J. Am. Ceram. Soc.*, 2014, **1**, 7.
8 N. Guo, Y. H. Zheng, Y. C. Jia, H. Qiao, H. P. You, *New J. Chem.*, 2012, **36**, 168.
9 M. B. Xie, Y. Tao, Y. Huang, H. B. Liang, Q. Su, *Inorg. Chem.*, 2010, **49**, 11317.
10 B. Han, H. B. Liang, H. Y. Ni, Q. Su, G. T. Yang, J. Y. Shi, G. B. Zhang, *Opt. Express*, 2009, **17**, 7138.
11 W. Lv, Y. C. Jia, W. Z. Lv, Q. Zhao, H. P. You, *New J. Chem.*, 2013, **37**, 3701.
12 J. H. Hao, M. Cocivera, *Appl. Phys. Lett.*, 2001, **79**, 740.
13 J. H. Hao, M. Cocivera, *Appl. Phys. Lett.*, 2002, **81**, 4154.
14 J. H. Hao, J. Gao, M. Cocivera, *Appl. Phys. Lett.*, 2003, **82**, 2778.
15 M. D. Que, Z. P. Ci, Y. H. Wang, G. Zhu, S. Y. Xin, Y. R. Shi, Q. Wang, *CrystEngComm*, 2013,**15**, 6389.
16 Z. P. Ci, M. D. Que, Y. R. Shi, G. Zhu, Y. H. Wang, *Inorg. Chem.*, 2014, **53**, 2195.
17 Z. J. Wang, P. L. Li, Q. L. Guo, Z. P. Yang, *Mater. Res. Bull.*, 2014, **52**, 30.
18 J. S. Kim, P. E. Jeon, J. C. Choi, *Appl. Phys. Lett.*, 2004, **84**, 2931.
19 K. H. Kwon, W. B. Im, H. S. Jang, *Inorg.Chem.*, 2009, **48**, 11525.
20 S. S. Sanayea, B. S. Dhabekar, *J. Lumin.*, 2003, **105**, 1.
21 J. Sokolnicki, *J. Phys.:Condens. Matter.*, 2010, **22**, 275301.
22 C. Chang and T. Chen, *Appl. Phys. Lett.*, 2007, **91**, 081902.
23 V. Sivakumar and U. V. Varadaraju, *J. Electrochem. Soc.*, 2009, **156**, 179.
24 C. Kulshreshtha, J. H. Kwak, Y. J. Park, *Opt. Lett.*, 2009, **34**, 794.
25 N. Suriyamurthy,B. S. Panigrahi, *J. Lumin.*, 2007, **127**, 483.
26 D. Hou, B. Han, W. P Chen, H. B. Liang, *J. Appl. Phys.*, 2010, **108**, 083527.
27 U. Caldin˜o, *J. Phys.: Condens. Matter.*, 2005, **17**, 7297.
28 S. H. Yang and N. J. Cheng, *J. Alloys Compd.*, 2010, **489**, 689.
29 Y.M. Pan, M.E. Fleet, *Rev. Mineral. Geochem.*, 2002, **48**, 13-49.
30 T.J. White, Z.L. Dong, *Acta Crystallogr.,Sect. B: Struct. Sci.*, 2003, **59**, 1-16.
31 T. White, C. Ferraris, J. Kim, S. Madhavi, *Rev. Mineral. Geochem.*, 2005, **57**, 307-401.
32 C. Calvo, R. Faggiani, *J. Chem. Soc., Chem. Commun.*, 1974, **1974**, 714-715.
33 C. Calvo, R. Faggiani, N. Krishnamachari, *Acta Crystallographica Section B*, 1975, *31*, 188-192.
34 S. Chen, S. Hoffmann, W. Carrillo-Cabrera, L. Akselrud, Y. Prots, U. Schwarz, J. T. Zhao, *J. Solid State Chem.*, 2010, **183**, 658-661.
35 H. K. Liu, Y. Luo, Z. Y. Mao, L. B. Liao, Z. G. Xia, *J. Mater. Chem. C*, 2014, **2**, 1619.
36 Y. Zhang, G. G. Li, D. L. Geng, M. M. Shang, C. Peng, J. Lin, *Inorg. Chem.*, 2012, **51**, 11655.
37 M. M. Shang, D. L. Geng, D. M. Yang, X. J. Kang, Y. Zhang, J. Lin, *Inorg. Chem.*, 2013, **52**, 3102.
38 L. G. Van Uitert, *J. Lumin.*, 1984, **29**, 1-9.
39 P. D. Rack and P. H. Holloway, *Mater. Sci. Eng. Rep.*, 1998, **21**, 171-219.
40 G. G. Li, D. L.Geng, D. M. Yang, X. J.Kang, Y. Zhang, H. Z.Lian, J. Lin, *J. Phys. Chem. C*., 2012, **116**, 10222-10231.
41 P. I. Paulose, G. Jose, V. Thomas, N. V. Unnikrishnan, M. K. R. Warrier, *J. Phys. Chem. Solids*, 2003, **64**, 841-846.
42 N. Guo, Y. J. Huang, H. P. You, M. Yang, Y. H. Song, K. Liu, Y. H. Zheng, *Inorg. Chem.*, 2010, **49**, 10907-10913.
43 C. H. Huang, T. W. Kuo, T. M. Chen, *ACS Appl. Mater. Interfaces*, 2010, **2**, 1395-1399.
44 F. P. Du, Y. Nakai, T. Tsuboi, Y. Huang, H. J. Seo, *J. Mater.Chem.*, 2011, **21**, 4669.
45 D. J. Dexter, *J. Chem. Phys.*, 1953, **21**, 836-850.
46 C. C.Lin, Z. R.Xiao, G. Y. Guo, T. S. Chan, R. S.Liu, *J. Am. Chem. Soc.*, 2008, **43**, 5658-5659.
47 X. Q.Piao, K. Machida,T. Horikawa, H.Hanzawa, Y. Shimomura, N. Kijima, *Chem. Mater.*, 2007, **19**, 4592-4599.
48 Y. Q. Li, N.Hirosaki, R. J. Xie, T. Takeda, M. Mitomo, *Chem. Mater.*, 2008, **20**, 6704-6714.
49 W. R. Liu, C. W. Yeh, C. H. Huang, C. C. Lin, Y. C. Chiu, Y.T. Yeh, R.S. Liu, *J. Mater. Chem.*, 2011, **21**, 3740-3744.
50 X. Q. Piao, T. Horikawa, H.Hanzawa, K.Machida, *Appl. Phys. Lett.*,2006. **88**, 161908-1-161908-3.

51 I. Baginskiy, R. S. Liu, C. L. Wang, R.T.Lin, J. Y.Yao, *J. Electrochem. Soc.*, 2011, **158**, 118-121.

The Structure, Photoluminescence and Thermal Properties of Ce^{3+}, Mn^{2+} Co-doped Phosphosilicate $Sr_7La_3[(PO_4)_{2.5}(SiO_4)_3(BO_4)_{0.5}](BO_2)$ Emission-Tunable Phosphor

Zhipeng Ci,[*a] Qisheng Sun[a], Mengxing Sun[a], Xiaojing Jiang[a], Shengchun Qin[a], Yuhua Wang[*a]

A single phase emission-tunable $Sr_7La_3[(PO_4)_{2.5}(SiO_4)_3(BO_4)_{0.5}](BO_2)$: Ce^{3+}, Mn^{2+} phosphor was synthesized and the photoluminescence, energy-transfer mechanism and thermal properties are carefully investigated.